Coastal Engineering, 11 (1987) 565–601
Elsevier Science Publishers B.V., Amsterdam — Printed in The Netherlands

Quasi-3D Modelling of Nearshore Currents

H.J. DE VRIEND and M.J.F. STIVE
Delft Hydraulics, 2600 MH Delft, The Netherlands
(Received October 10, 1986; revised and accepted March 11, 1987)

ABSTRACT

De Vriend, H.J. and Stive, M.J.F., 1987. Quasi-3D modelling of nearshore currents. In: P.P.G. Dyke (Editor), JONSMOD '86. *Coastal Eng.*, 11: 565–601.

Existing concepts of wave-induced nearshore current models, in the cross-shore vertical plane (2DV) and depth-integrated (2DH), are combined to a quasi-3D mathematical model. This combination is tested for reproducing correct results in 2DV and 2DH situations. The importance of the various contributions to the wave-induced secondary circulation in the vertical plane is investigated for realistic parameter ranges, which leads to the conclusion that both the non-breaking and the breaking fraction of a random wave field in the surf zone generate important secondary currents.

Additional computations show the relevance of a 3D-approach of nearshore currents, even in seemingly simple situations like a plane sloping beach with obliquely incident waves.

INTRODUCTION

The physical understanding and the mathematical modelling of hydrodynamical processes in the nearshore zone are of increasing interest, not only to coastal engineering and coastal zone management, but also to many other disciplines, such as oceanography of shallow seas, ecology and geology. The last two decades have brought substantial progress at these points, in the modelling of short waves (generation, propagation, dissipation) as well as in the modelling of complex tidal and wave-induced currents. Also the understanding and modelling of coastal sediment transport have made an important step foreward in this period.

As a result of these developments, the mathematical modelling of coastal morphology has come within reach and various institutes all over the world are developing such models now. So far, most of these models are formulated in a single vertical plane (Bailard, 1982; Dally and Dean, 1984; Swain and Houston, 1984; Stive and Battjes, 1984; Stive, 1985, 1986) or in terms of depth-integrated quantities (Fleming and Hunt, 1976; Coeffé and Péchon, 1982; McAnally et al., 1984; De Vriend, 1986a). Only very few take account of the

0378-3839/87/$03.50

spatially three-dimensional character of the phenomena (Farmer and Waldrop, 1977; Koutitas et al., 1985; McAnally et al., 1986; also see De Vriend, 1986b).

At present it seems as though mathematical models in two spatial dimensions, either horizontal or in the vertical plane, are not sufficient for many practical applications. The integration of these two classes of models, and eventually a new generation of fully 3D models is needed. As a first step towards this integration, a quasi-3D model of nearshore currents is developed, on the basis of existing concepts of 2DH (horizontal plane) and 2DV (vertical plane) current models. The results is a combination of a depth-integrated model and a vertical profile technique.

MORPHOLOGICAL COMPUTATION PROCEDURE

Before going into the specific aspects of 3D wave and current models, they are put into the context of a combined morphological computation procedure. To that purpose an aggregate flow chart is given in Fig. 1.

The principal assumptions underlying the computation procedure are:
- a one-way interaction between the components of the model, as indicated in the flow chart; and
- applicability of a vertical similarity approximation to all 3D-dependent variables in the system.

In terms of the computational algorithm, the former assumption implies that each constituent model can be run with the results from the other models as fixed parameters and that the modules in Fig. 1 can be treated one by one in the indicated sequence. Hence, this procedure is a generalization of the so-called quasi-steady computation procedure, a very common approach in morphological models.

For the wave motion, the assumptions imply that the mild-slope approximation applies (Berkhoff, 1976) and that current refraction can be disregarded or modelled using a rough estimate of the current field. For the time-mean current they imply that it is nearly horizontal and that the shallow-water approximation applies.

The consequences of these assumptions are given further attention in the next sections, where the wave module is discussed briefly and the net current modules are presented in detail.

THE WAVE MODULE

There is a wide variety of mathematical models describing the generation, propagation and dissipation of waves in the coastal zone, so there seems to be a choice of possibilities to fill in the wave module. Each model, however, has been developed and tested primarily for separate application, i.e. to provide

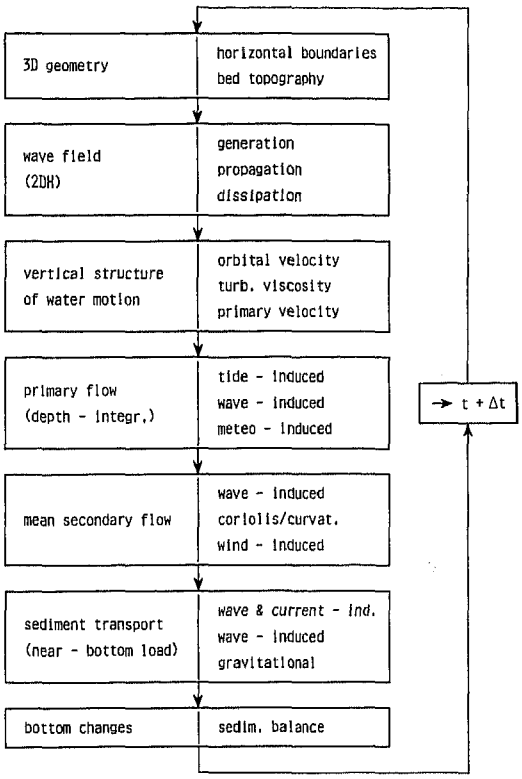

Fig. 1. Aggregate flow chart.

final results that are not processed in a subsequent chain of models. In a compound model like the present one, the wave model is subject to specific requirements, such as:

- the need of different output quantities (e.g. the wave-induced driving forces and the near-bottom orbital velocity);
- a sufficient numerical accuracy of the results, to stand their further processing (involution, numerical differentiation); and
- it must not give rise to spurious interactions with the other models, neither physical, nor numerical.

Consequently, caution has to be exercised in selecting the wave model (cf. De Vriend, 1985b; Dingemans et al., 1987).

For the kind of morphological models concerned here, it is not yet quite clear how these requirements work out. Current research at Delft Hydraulics, on the interaction of the modules in a morphological model without secondary flow (De Vriend, 1986b), indicates that some degree of diffraction is needed in the wave model, in order to obtain realistic results. The picture is still incomplete, however, and a lot of work remains to be done in the complicated field of model

interactions. For the time being, a trial-and-error procedure seems to be the only feasible approach.

A reasonable first shot for nearshore applications seems to be a wave model without energy production by wind input or dissipation by bottom friction, with propagation based on linear wave theory and with breaking-induced dissipation formulated according to Battjes and Janssen (1978). The latter formulation has proved quite useful in nearshore current models (Dingemans et al., 1987) and in cross-shore morphological models (Stive and Battjes, 1984; Stive, 1985, 1986). Theoretically, the wave-induced driving forces can be derived from the radiation stress gradients. A numerically and physically more robust and transparent formulation, however, relates the force to the energy dissipation rate. It was first mentioned by Longuet-Higgins (1970) and Battjes (1974) for refracting wave fields. Its validity for wave fields with refraction and diffraction was recently shown by Dingemans et al. (1987).

NEARLY HORIZONTAL WAVE- AND TURBULENCE-AVERAGED FLOW

The starting point of the current model are the Reynoldfs equations for turbulence-averaged flow. If, apart from the wave-induced orbital motion, the current involves no strong vertical accelerations, the time-mean pressure can be approximated by:

$$p \approx p_h - \rho \langle \tilde{w}^2 \rangle \tag{1}$$

in which

p = pressure,
p_h = hydrostatic pressure,
ρ = mass density of the fluid,
$\tilde{w}$ = vertical component of the wave orbital velocity,
$\langle .. \rangle$ = average over the waves.

If, in addition, the Boussinesq-hypothesis is adopted to model the Reynolds stress terms, the wave- and turbulence-averaged horizontal momentum equations can be written as:

$$\frac{\partial u}{\partial t} + u\frac{\partial u}{\partial x} + v\frac{\partial u}{\partial y} + w\frac{\partial u}{\partial z} - f_c v = -\frac{1}{\rho}\frac{\partial p_n}{\partial x} + \frac{\partial}{\partial x}\left(\nu_t \frac{\partial u}{\partial x}\right) + \frac{\partial}{\partial y}\left(\nu_t \frac{\partial u}{\partial y}\right) + \frac{\partial}{\partial z}\left(\nu_t \frac{\partial u}{\partial z}\right)$$
$$- \frac{\partial}{\partial x}(\langle \tilde{u}^2 \rangle - \langle \tilde{w}^2 \rangle) - \frac{\partial}{\partial y}(\langle \tilde{u}\tilde{v} \rangle) - \frac{\partial}{\partial z}(\langle \tilde{u}\tilde{w} \rangle) \tag{2}$$

$$\frac{\partial v}{\partial t} + u\frac{\partial v}{\partial x} + v\frac{\partial v}{\partial y} + w\frac{\partial v}{\partial z} + f_c u = -\frac{1}{\rho}\frac{\partial p_n}{\partial y} + \frac{\partial}{\partial x}\left(\nu_t \frac{\partial v}{\partial x}\right) + \frac{\partial}{\partial y}\left(\nu_t \frac{\partial v}{\partial y}\right) + \frac{\partial}{\partial z}\left(\nu_t \frac{\partial v}{\partial z}\right)$$
$$- \frac{\partial}{\partial x}(\langle \tilde{u}\tilde{v} \rangle) - \frac{\partial}{\partial y}(\langle \tilde{v}^2 \rangle - \langle \tilde{w}^2 \rangle) - \frac{\partial}{\partial z}(\langle \tilde{v}\tilde{w} \rangle) \tag{3}$$

with

x, y = horizontal co-ordinates in a cartesian system,
z = vertical co-ordinate in this system,
u, v, w = wave- and turbulence-mean velocity components,
p_n = $p_h + \rho g(z - \langle z_s \rangle)$ = total hydrostatic pressure,
f_c = coriolis coefficient
g = acceleration due to gravity,
$\langle z_s \rangle$ = mean water level,
ν_t = turbulence viscosity (eddy viscosity),
$\tilde{u}, \tilde{v}$ = horizontal components of the wave orbital velocity.

Together with the corresponding equation of continuity:

$$\frac{\partial u}{\partial x} + \frac{\partial v}{\partial y} + \frac{\partial w}{\partial z} = 0 \tag{4}$$

these equations describe the wave- and turbulence-averaged current, which may still be time-dependent on a time-scale much larger than the wave period or the time-scale of turbulence.

Equations (2) and (3) include one other assumption, which can be explained as follows. Let the instantaneous velocity component U be given by:

$$U = u + \tilde{u} + u' \tag{5}$$

in which u' denotes the turbulent velocity fluctuation, then it is assumed that:

$$\langle U^2 \rangle = u^2 + \langle \tilde{u}^2 \rangle + \langle u'^2 \rangle \tag{6}$$

This means that turbulence and wave motion are assumed to be uncorrelated. In view of the "first-shot" approach, this seems reasonable for a combination of waves and currents.

Outside the bottom boundary layer, the last term in either momentum equation is neglected with regard to the corresponding Reynolds stress term, since the horizontal and vertical velocity components of the orbital velocity are approximately 90 degrees out of phase, whereas the turbulent velocity components are much less so.

SIMILARITY APPROACH

The basic idea of the current model is a similarity approach, assuming that each dependent variable can be written in the form:

$$u = \sum_i \tilde{u}_i(x,y,t) f_i\left(\frac{z - z_b}{h}\right) \tag{7}$$

in which z_b denotes the bottom level and h the water depth for $z_s = \langle z_s \rangle$. The

quantity $\bar{u}_i$ is independent of z and the vertical distribution function f_i is invariant, or at most weakly varying, with x and y.

If the series in eqn. (7) would be extended to an infinite number of terms, this approach would correspond with the formal separation of variables. In the present model, it is attempted to define the constituents in such a way, that a truncated series of only a few terms yields a good approximation of the solution.

The dependent variables in the current model are the pressure p_n (or the mean water surface elevation $\langle z_s \rangle$) and the velocity components u, v and w. Besides, the system requires a turbulence closure, relating ν_t to the velocity field.

The series (7) for the total hydrostatic pressure simply reduces to:

$$p_n = p_n(x,y,t) \tag{8}$$

which reflects the assumption of hydrostaticity.

The current is split into what will be called a "primary" and a "secondary" current, according to the definition:

$$u = u_p + u_s \quad \text{with} \quad u_p = \bar{u}(x,y,t) f_p\left(\frac{z-z_b}{h}\right) \quad \text{and} \quad \bar{u}_s = 0 \tag{9}$$

$$v = v_p + v_s \quad \text{with} \quad v_p = \bar{v}(x,y,t) f_p\left(\frac{z-z_b}{h}\right) \quad \text{and} \quad \bar{v}_s = 0 \tag{10}$$

in which the suffix p denotes the primary current, the suffix s the secondary current and the overbar the depth-averaged value. So, by definition, the depth-averaged flow is determined entirely by the primary current.

It has to be noted that the definitions (9) and (10) are not unique, as long as the vertical distribution function f_p is not specified. Besides, u_s and v_s remain to be written as a similarity series like eqn. (7). These points will be considered in the next sections.

Once the horizontal components of the primary and the secondary flow velocity have been defined, the vertical components follow from the equation of continuity (4):

$$\frac{\partial w_p}{\partial z} = -\frac{\partial u_p}{\partial x} - \frac{\partial v_p}{\partial y} \quad \text{and} \quad \frac{\partial w_s}{\partial z} = -\frac{\partial u_s}{\partial x} - \frac{\partial v_s}{\partial y} \tag{11}$$

For simplicity, an algebraic turbulence closure is adopted, relating ν_t algebraically to the local flow velocity. Besides, ν_t is assumed to be described by the one-term similarity "series":

$$\nu_t = \bar{\nu}_t(x,y,t)\ \phi\left(\frac{z-z_b}{h}\right) \tag{12}$$

in which the depth-average $\bar{\nu}_t$ and the vertical distribution function ϕ remain to be specified.

TURBULENCE MODEL

The Boussinesq hypothesis combined with an algebraic relationship between the turbulence viscosity and the flow velocity has often been applied with success in models of large-scale steady or slowly varying flow in shallow water. In coastal models, the presence of short waves and their effects on the turbulent exchange of momentum have to be taken into account.

Compared with the steady flow case, the principal short-wave effects are:
- an increase of the turbulence production and the eddy viscosity, due to the wave orbital motion; and
- if the waves are breaking: an increase of the turbulence production and the eddy viscosity.

Investigations of the near-bottom velocity distribution for combinations of waves and currents have led various authors (Lundgren, 1972; Grant and Madsen, 1979; Asano and Iwagaki, 1984; Coffey and Nielsen, 1984; Van Kesteren and Bakker, 1984) to essentially the same concept of incorporating the wave effects on the mean current velocity. The velocity distribution is modelled as if there were no waves, only the bottom roughness length, is given a higher value to account for the velocity reduction in the wave boundary layer. So the eddy viscosity distributions commonly applied in steady or weakly varying flow models can be utilized here, as well.

It has to be noted that, in terms of the present definitions, this concept pertains only to the primary velocity outside the wave boundary layer. If the mean velocity inside this layer has to be described, the eddy viscosity has to be adjusted there. As a first approximation, Coffey and Nielsen (1984) propose a constant value of ν_t in a part of the wave boundary layer:

$$\nu_t = \kappa u_* \delta (1 - \delta/h) \quad \text{for} \quad z - z_b < \delta \tag{13}$$

in which κ is Von Karman's constant and u_* is the current friction velocity.

The possibly enhanced vertical mixing due to the wave orbital motion is assumed not to affect the vertical distribution function of the eddy viscosity, but only its depth-averaged value. In most models, the increase of $\bar{\nu}_t$ is incorporated via the increase of the current friction velocity u_*:

$$\bar{\nu}_t = K u_* h \tag{14}$$

in which K is a constant that remains to be determined.

Breaking waves give rise to an additional production of turbulence. Starting from the similarity of the flow in a spilling breaker with that in a wake, Stive and Wind (1986) estimate the eddy viscosity in the region below the trough level in breaking waves without a primary current at $0.01\,ch$, where c denotes the celerity of the waves. The authors explicitly state, however, that on the basis of the available data they are not able to specify the vertical distribution

of ν_t, so that their estimate rather pertains to the effect of wave breaking on $\bar{\nu}_t$. On the other hand, Battjes (1983) proposes to relate the horizontal diffusion coefficient in wave-driven current computations to the mean rate of wave-energy dissipation per unit area, D:

$$\bar{\nu}_h = M_h h (D/\rho)^{1/3} \tag{15}$$

in which M_h is a constant, supposed to be of the order O(1) (also see Visser, 1984).

For the present model, which has to cover combinations of breaking waves and strong currents, expressions (14) and (15) for $\bar{\nu}_t$ have to be combined and the vertical distribution function ϕ has to be specified. By lack of further information, a more or less heuristic approach is chosen. The separate eddy viscosities due to currents and breaking waves are simply added, to yield:

$$\bar{\nu}_t = K u_* h + M h (D/\rho)^{1/3} \tag{16}$$

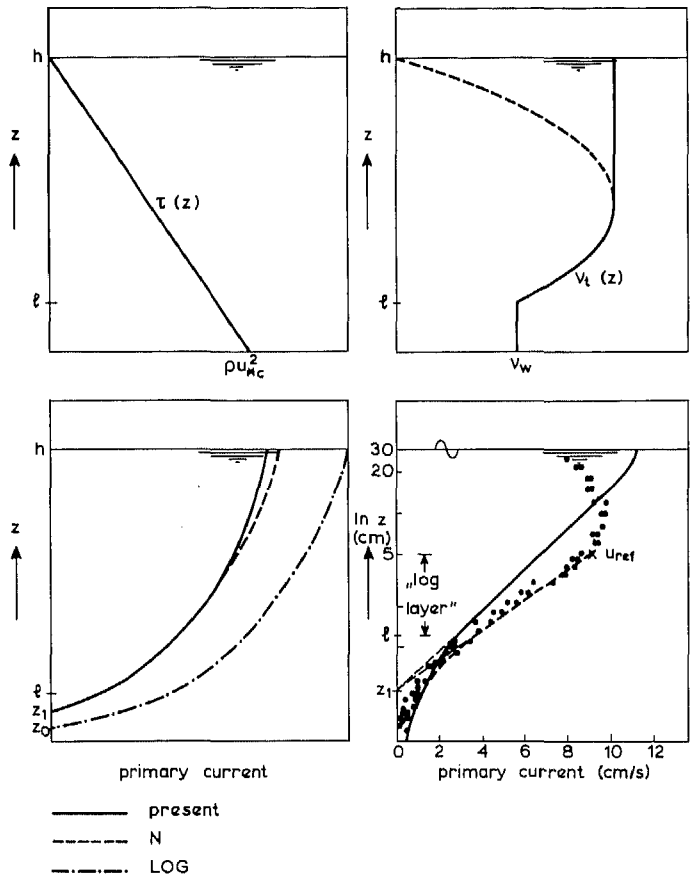

Fig. 2. Vertical distributions of shear stress, turbulence and primary velocity. Data points: measured values (after Van Doorn, 1981). Curves: several theories, see legend; *LOG* is usual logarithmic model, *N* is Nielsen's (1985) model and *present* is present model.

in which M is a constant, not necessarily equal to M_h. A theoretical basis to assess the correct value of M is still lacking; a pragmatic choice of 0.025 is discussed in a next section.

The assessment of the vertical distribution function is based on the following observations:

- the turbulence production by spilling breakers is strongest in the upper part of the vertical (Stive and Wind, 1982);
- the primary velocity distribution is fairly insensitive to the vertical distribution of ν_t in the upper part of the vertical (De Vriend, 1981); and
- the wave-induced undertow (Stive and Wind, 1986), but also other types of secondary flow, e.g. curvature-induced (De Vriend, 1981) or coriolis-induced (Kalkwijk and Booij, 1986), are described fairly well with a constant eddy viscosity in the upper part of the vertical.

Hence, a constant eddy viscosity for $z-z_b > \frac{1}{2}h$ seems to be appropriate as a first guess.

The resulting turbulence model consists of eqns. (12) and (14), with the vertical distribution function (also see Fig. 2):

$$\phi(\zeta) = \begin{cases} \phi|_{\zeta=F\zeta_0} & \text{for } 0<\zeta\leqslant F\zeta_0 \\ \phi(\zeta)|_{\text{current}} & \text{for } F\zeta_0\leqslant\zeta\leqslant\frac{1}{2} \\ \phi|_{\zeta=\frac{1}{2}} & \text{for } \zeta\geqslant\frac{1}{2} \end{cases} \tag{17}$$

in which $\zeta=(z-z_b)/h$ is the normalized vertical coordinate and F is the bottom roughness amplification factor (Nielsen, 1985), which is a function of the near-bottom orbital velocity, the current velocity, etc. Its specification is given in the next section.

DIVISION OF THE FLOW EQUATIONS

Substitution of the definitions (9) and (10) into the x-momentum equation (2) yields:

$$\begin{aligned} &\frac{\partial u_p}{\partial t}+u_p\frac{\partial u_p}{\partial x}+v_p\frac{\partial u_p}{\partial y}+w_p\frac{\partial u_p}{\partial z}-f_c v_p+\frac{\partial u_s}{\partial t}+u_s\frac{\partial u_s}{\partial x}+v_s\frac{\partial u_s}{\partial y}+w_s\frac{\partial u_s}{\partial z} \\ &\quad -f_c v_s+u_s\frac{\partial u_p}{\partial x}+v_s\frac{\partial u_p}{\partial y}+w_s\frac{\partial u_p}{\partial z}+u_p\frac{\partial u_s}{\partial x}+v_p\frac{\partial u_s}{\partial y}+w_p\frac{\partial u_s}{\partial z}= \\ &\quad -\frac{1}{\rho}\frac{\partial p_n}{\partial x}-\frac{\partial}{\partial x}\left(\nu_t\frac{\partial u_p}{\partial x}\right)+\frac{\partial}{\partial y}\left(\nu_t\frac{\partial u_p}{\partial y}\right)+\frac{\partial}{\partial z}\left(\nu_t\frac{\partial u_p}{\partial z}\right)+\frac{\partial}{\partial x}\left(\nu_t\frac{\partial u_s}{\partial x}\right) \\ &\quad +\frac{\partial}{\partial y}\left(\nu_t\frac{\partial u_s}{\partial y}\right)+\frac{\partial}{\partial z}\left(\nu_t\frac{\partial u_s}{\partial z}\right)-\frac{\partial}{\partial x}(\langle\tilde{u}^2\rangle-\langle\tilde{w}^2\rangle)-\frac{\partial}{\partial y}(\langle\tilde{u}\tilde{v}\rangle) \end{aligned} \tag{18}$$

Substitution into the y-momentum equation (3) yields a similar result. Inte-

gration of eqn. (18) from the bottom to a point above the highest water surface elevation yields, after some elaboration:

$$\frac{\partial \bar{u}}{\partial t}+\overline{f_p^2}\left(\bar{u}\frac{\partial \bar{u}}{\partial x}+\bar{v}\frac{\partial \bar{u}}{\partial y}\right)-f_c\bar{v}+\frac{1}{h}\left[\frac{\partial}{\partial x}\right](h\overline{u_s^2})+\frac{\partial}{\partial y}\left[(h\overline{u_s v_s})\right]$$
$$+\frac{1}{h}\left[\frac{\partial}{\partial x}\right](h\overline{u_p u_s})+\frac{\partial}{\partial y}\left[(h\overline{u_p v_s})\right]+\frac{1}{h}\left[\frac{\partial}{\partial x}\right](h\overline{u_s u_p})+\frac{\partial}{\partial y}\left[(h\overline{u_s v_p})\right]=$$
$$-\frac{1}{\rho}\frac{\partial p_n}{\partial x}+\overline{\frac{\partial}{\partial x}\left(\nu_t\frac{\partial u_p}{\partial x}\right)}+\overline{\frac{\partial}{\partial y}\left(\nu_t\frac{\partial u_p}{\partial y}\right)}+\overline{\frac{\partial}{\partial x}\left(\nu_t\frac{\partial u_s}{\partial x}\right)}+\overline{\frac{\partial}{\partial y}\left(\nu_t\frac{\partial u_s}{\partial y}\right)}$$
$$-\frac{\tau_{bp_x}}{\rho h}-\frac{\tau_{bs_x}}{\rho h}-\frac{1}{\rho h}\left(\frac{\partial S_{xx}}{\partial x}+\frac{\partial S_{xy}}{\partial y}\right)+\frac{W_x}{\rho h} \qquad (19)$$

in which τ_{bp_x} and τ_{bs_x} are the bottom shear stress components related to the primary and the secondary flow, respectively, and W_x is the x-component of the wind shear stress at the water surface. S_{xx} and S_{xy} are components of the radiation stress, defined as (Battjes, 1974):

$$S_{xx}=\int_{z_b}^{\langle z_s\rangle}\rho(\langle\tilde{u}^2\rangle-\langle\tilde{w}^2\rangle)\,dz+\tfrac{1}{2}\rho g\langle(z_s-\langle z_s\rangle)^2\rangle \quad \text{and}$$
$$S_{xy}=\int_{z_b}^{\langle z_s\rangle}\langle\rho\tilde{u}\tilde{v}\rangle\,dz \qquad (20)$$

Elimination of the pressure gradient term from eqns. (18) and (19) leads to an equation that can be elaborated to:

$$\frac{\partial}{\partial z}\left(\nu_t\frac{\partial u_p}{\partial z}\right)+\frac{\tau_{bp_x}}{\rho h}+\frac{\partial}{\partial z}\left(\nu_t\frac{\partial u_s}{\partial z}\right)+\frac{\tau_{bs_x}}{\rho h}+f_c v_s=$$
$$\frac{W_x}{\rho h}+\frac{\partial}{\partial x}(\langle\tilde{u}^2\rangle-\langle\tilde{w}^2\rangle)-\frac{1}{\rho h}\frac{\partial S_{xx}}{\partial x}+\frac{\partial}{\partial y}(\langle\tilde{u}\tilde{v}\rangle)-\frac{1}{\rho h}\frac{\partial S_{xy}}{\partial y}$$
$$+(f_p-1)\left(\frac{\partial \bar{u}}{\partial t}-f_c\bar{v}\right)+(f_p^2-\overline{f_p^2})\left(\bar{u}\frac{\partial \bar{u}}{\partial x}+\bar{v}\frac{\partial \bar{u}}{\partial y}\right)+\text{other terms} \qquad (21)$$

The "other terms" in this equation concern the vertical non-uniformity of the advection of secondary flow momentum by the primary and the secondary current, the advection of primary flow momentum by the secondary current and the horizontal diffusion of primary and secondary flow momentum. For the time being, all these terms will be disregarded.

Equation (21) is used for a further specification of the primary and the secondary current. The primary current is defined such, that:

$$\frac{\partial}{\partial z}\left(\nu_t \frac{\partial u_p}{\partial z}\right)+\frac{\tau_{bp_x}}{\rho h}=0 \tag{22}$$

which implies that it is driven by the depth-invariant part of the forces (pressure gradient, depth-averaged wave-induced force, depth-averaged wind force).

The direction of the primary bottom shear stress is assumed to coincide with the depth-averaged flow direction. Hence, eqn. (22) describes the vertical distribution function of the primary flow and establishes the relationship between the primary bottom shear stress and the depth-averaged velocity. This makes the y-equivalent of this equation redundant.

Substitution of eqn. (22) into eqn. (21) leads to the following equation for the secondary flow:

$$\frac{\partial}{\partial z}\left(\nu_t \frac{\partial u_s}{\partial z}\right)+\frac{\tau_{bs_x}}{\rho h}+f_c v_s=\frac{W_x}{\rho h}+\frac{\partial}{\partial x}(\langle \tilde{u}^2\rangle-\langle \tilde{w}^2\rangle)-\frac{1}{\rho h}\frac{\partial S_{xx}}{\partial x}$$
$$+\frac{\partial}{\partial y}(\langle \tilde{u}\tilde{v}\rangle)-\frac{1}{\rho h}\frac{\partial S_{xy}}{\partial y}+\left(f_p-1\right)\left(\frac{\partial \bar{u}}{\partial t}-f_c\bar{v}\right)+\left(f_p^2-\overline{f_p^2}\right)\left(\bar{u}\frac{\partial \bar{u}}{\partial x}+\bar{v}\frac{\partial \bar{u}}{\partial y}\right) \tag{23}$$

According to this equation, there are four sources of secondary flow, viz.:

- the wind shear stress at the water surface, which gives rise to a current velocity with a vertical distribution that deviates from the primary current distribution and, if the coriolis-effect is important, even to a velocity direction that varies along the vertical (Ekman, 1905; also see Memos, 1985; Davies, 1987; Jenkins, 1987); in the present concept, the deviations from the fictitious velocity obtained by multiplying the depth-averaged wind-induced current velocity with the primary velocity distribution function f_p are considered as secondary flow;
- the vertical non-uniformity of the wave-induced forces, related to the mass flux above the wave through level and the return flow or undertow below this level (Dyhr-Nielsen and Sørensen, 1970; Stive and Wind, 1986);
- the vertical non-uniformity of the main flow acceleration, in time and due to the coriolis-effect (also see Kalkwijk and Booij, 1986);
- the vertical non-uniformity of the advective accelerations of the main flow, including the well-known curvature-induced secondary flow (Boussinesq, 1868), but also the deformation of the current profile due to downstream accelerations (De Vriend, 1977).

In complex coastal areas, each of these secondary currents can have an important effect on the morphological evolution. Therefore, each of them deserves full attention when developing a mathematical model of coastal morphology. Practical restrictions, however, allow for the evaluation of only one of them, viz. the wave-induced secondary flow. In fact, this means that attention is focused on the surf zone of a nearly uniform coast, although the formulations will be so general, that they basically allow for more complex situations.

Without stating this explicitly, the secondary flow velocity was and will be assumed small compared with the primary one, e.g. when neglecting the "other terms" in eqn. (21). This has to be kept in mind, especially when considering the wind- and wave-induced currents, which can occur with a zero primary velocity.

PRIMARY CURRENT

Vertical distribution of the primary velocity

With the similarity hypotheses (9), (10) and (12), eqn. (22) and its y-equivalent can be rewritten to:

$$\frac{\partial}{\partial\zeta}\left(\phi\frac{\partial f_p}{\partial\zeta}\right)=-C_\tau \quad \text{with} \quad C_\tau=\frac{\tau_{bpx}h}{\rho\bar{\nu}_t\bar{u}}=\frac{\tau_{bpy}h}{\rho\bar{\nu}_t\bar{v}} \tag{24}$$

Together with the boundary conditions:

$$f_p\,|_{\zeta=F'\zeta_o}=0 \quad \text{and} \quad \left|\phi\frac{\partial f_p}{\partial\zeta}\right|_{\zeta=1}=0 \tag{25}$$

and the requirement $\bar{f}_p=1$ (by definition), this equation describes the vertical distribution function f_p and the constant C_τ, which establishes the relation between the primary bottom shear stress and the depth-averaged velocity.

Elaboration for a parabolic distribution of $\phi(\zeta)$ in the lower half of the water column (see eqn. (17) and Fig. 2) yields, after some algebra and with $F'=F\exp(F^{-1}-1)$, according to Nielsen (1985):

$$f_p=\begin{cases}-\dfrac{3}{1+3\ln(2F'\zeta_o)}[\ln\zeta-\ln(F'\zeta_o)] & \text{for } F\zeta_o\leqslant\zeta\leqslant\frac{1}{2}\\[2ex] -\dfrac{3}{1+3\ln(2F'\zeta_o)}[-2\zeta^2+4\zeta-\dfrac{3}{2}-\ln(2F'\zeta_o)] & \text{for } \frac{1}{2}\leqslant\zeta\leqslant 1\end{cases} \tag{26}$$

$$C_\tau=-\frac{24}{5}\frac{3}{1+3\ln(2F'\zeta_o)} \tag{27}$$

Note that f_p and C_τ are functions of x and y if $\ln(F'\zeta_o)$ is. Compared with the variations of the depth-averaged velocity, however, these quantities are assumed to vary only weakly in space.

A typical example of the primary velocity distribution according to eqn. (26) is given in Fig. 2, together with the usual logarithmic profile and measurements by Van Doorn (1981). Apparently, the distribution function (26) is not worse than the logarithmic one and agrees rather well with the measured data in what Coffey and Nielsen (1984) call the 'log-layer' of the flow. In their paper, Coffey and Nielsen give a logarithmic velocity profile that agrees far better with the

measured data than the profile labelled "present model" in Fig. 2. It has to be noted, however, that the constant of proportionality in their profile is the measured velocity at $0.2\,h$, instead of the imposed depth-averaged velocity (also see Neilsen, 1985). Thus the influence of the discrepancy between measured and calculated results in the upper half of the water column is eliminated.

The cause of the velocity reduction near the water surface is not quite clear, but evidently it cannot be described with a 2DV steady current model using a scalar turbulence viscosity, unless there is a negative effective shear stress near the surface. As the major part of the sediment transport takes place in the lower half of the water column, the results of the present model are acceptable as a basis for the computation of the magnitude of the sediment transport by the primary flow and the transport direction for a combination of a primary flow and a wave-induced secondary flow.

However, if the secondary flow depends on the primary velocity profile, like in the case of curvature- and coriolis-induced flows, this profile has to be correct throughout the water column. In cases where these types of secondary flow are important, the present model results may be unacceptable.

Bottom shear stress

Making use of eqns. (16), (24) and (27), the relation between the bottom shear stress and the depth-averaged velocity can be elaborated to:

$$\frac{\tau_{bp}}{\rho} \approx C_\tau \frac{\bar{u}_{tot}}{h}\left[Kh\left(\frac{\tau_{bp}}{\rho}\right)^{1/2} + Mh\left(\frac{D}{\rho}\right)^{1/3} \right] \quad \text{with} \quad \bar{u}_{tot} = (\bar{u}^2 + \bar{v}^2)^{1/2} \tag{28}$$

If there are no waves, this expression should change into the Chézy-formulation, i.e.:

$$\frac{g}{C^2}\bar{u}_{tot}^2 = C_\tau \bar{u}_{tot} K \frac{\sqrt{g}}{C}\bar{u}_{tot} \tag{29}$$

in which C denotes Chézy's factor. Elaboration of this expression, together with eqn. (27) for $F=1$ and $\zeta_o = \exp(-1-\kappa C g^{-\frac{1}{2}})$, yields:

$$K = \frac{5}{24}\kappa\left[1 + \left(\frac{2}{3} - \ln 2\right)\frac{\sqrt{g}}{\kappa C}\right] \approx \frac{5}{24}\kappa \tag{30}$$

This value of K is assumed invariant for all combinations of waves and currents.

If there are only non-breaking waves, eqn. (28) reduces to:

$$\left(\frac{\tau_{bp}}{\rho}\right)^{1/2} \approx K\, C_\tau\, \bar{u}_{tot} \tag{31}$$

Note that this is not necessarily an explicit expression in τ_{bp}, as C_τ depends on

the bottom roughness amplification factor F, which in turn may be a function of τ_{bp} (e.g. see Van Kesteren and Bakker, 1984).

If Nielsen's (1985) formulation is adopted, i.e.:

$$F \approx 1+\frac{1}{6}\left(\frac{U_{*w}}{U_{*c}}\right)^3 \tag{32}$$

where U_{*w} is the friction velocity that would be experienced by the pure wave motion and U_{*c} is the friction velocity for the mean current only, eqn. (31) is explicit in τ_{bp}. However, without further measures this formulation leads to a degeneration of the model for very high values of U_{*w}/U_{*c}. As such high values will occur in practical situations, F' will be given an upper bound. Limiting the effective bottom roughness to the thickness of the wave boundary layer, this upper bound follows from:

$$F'_{max}=\frac{C_f}{\omega}\frac{\bar{U}_{orb}}{h\zeta_o} \tag{33}$$

in which C_f is the bottom friction factor for the wave motion ($U_{*w}=C_f^{1/2}\bar{U}_{orb}$), ω is the angular frequency of the waves and $\bar{U}_{orb}$ is the amplitude of the near-bottom orbital velocity.

The validity of eqn. (28), including the effects of breaking waves, can be tested by comparing the results of a longshore current computation for a uniform coast with measurement by Thornton and Guza (1986), taken at Leadbetter Beach, Santa Barbara, California, as part of the NSTS-project. Figure 3 shows the beach profile and the measured wave heights and longshore current velocities, compared with the wave height distribution computed with the Battjes and Stive (1985) wave dissipation model ($\alpha=5, \gamma=0.4$) and the longshore current distributions obtained on the basis of these computed wave heights from:

- the model proposed by Battjes (1974), with linear bottom friction and disregarding lateral mixing, with $C_f=0.023$;
- the model proposed by Thornton and Guza (1985), based on the same assumptions and estimating the amplitude of the near-bottom orbital velocity with a long-wave formula, with $C_f=0.023$;
- the present model, with $M=0.025$.

For the measurement series considered here (Feb.4), the various longshore current distributions are not far apart and in good agreement with the measured data. Besides, additional numerical experiments made clear, that the computed longshore current distributions are much more sensitive to the wave height distribution than to their mutual differences. This means that, from a uniform longshore current point of view, the present model agrees well with commonly applied specific models.

The parameters C_f in the linear friction models and M in the present model

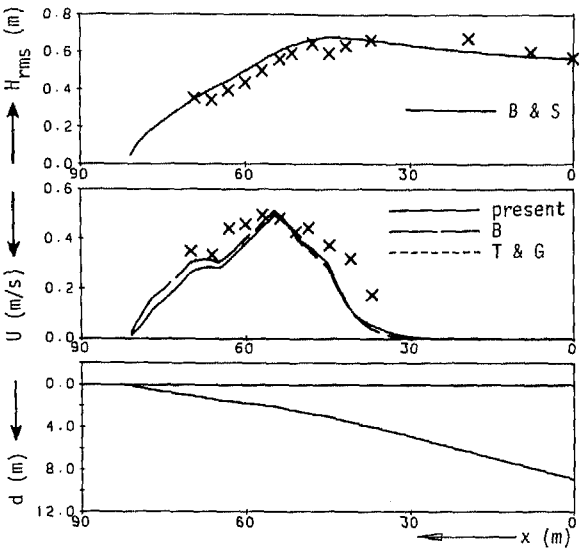

Fig. 3. Results for NSTS-campaign Feb. 4, 1980 at Leadbetter beach (measurements after Thornton and Guza, 1986); profiles of bottom elevation below MSL (d), longshore current (v), and rms wave height (H_{rms}) versus distance normal to shore (x). Data points: measured values. Curves: computations with the several models, see legend; *B & S* is Battjes and Stive (1985), *present* is present model, *B* is Battjes (1974), and *T & G* is Thornton and Guza (1986).

were adjusted to obtain a good fit with the measured data. The value of C_f is somewhat higher than expected from the grain roughness. The parameter M can be considered as indicating the fraction of the breaking-induced turbulence kinetic energy that penetrates below the trough level. The small value of this parameter corresponds well with the findings of Svendsen (1986).

Depth-averaged velocity field

Leaving all terms concerning the secondary flow out of consideration and adopting a Boussinesq hypothesis for the depth-averaged horizontal diffusion terms, eqn. (19) can be elaborated to:

$$\frac{\partial \bar{u}}{\partial t}+\overline{f_p^2}\left(\bar{u}\frac{\partial \bar{u}}{\partial x}+\bar{v}\frac{\partial \bar{u}}{\partial y}\right)-f_c\bar{v}=-\frac{1}{\rho}\frac{\partial p_n'}{\partial x}+\frac{1}{h\partial x}\left(\bar{\nu}_t h\frac{\partial \bar{u}}{\partial x}\right)+\frac{1}{h}\frac{\partial}{\partial y}\left(\bar{\nu}_t h\frac{\partial \bar{u}}{\partial y}\right)$$
$$-\frac{C_\tau \bar{\nu}_t}{h^2}\bar{u}+\frac{F_x}{\rho h}+\frac{W_x}{\rho h} \qquad (35)$$

in which p_n' is an approximation of the total hydrostatic pressure (an unknown) and F_x denotes the x-component of the depth-averaged wave-induced force per unit area.

Together with the corresponding equation in the y-direction:

$$\frac{\partial \bar{u}}{\partial t}+\overline{f_p^2}\left(\bar{u}\frac{\partial \bar{v}}{\partial x}+\bar{v}\frac{\partial \bar{v}}{\partial y}\right)+f_c\bar{u}=-\frac{1}{\rho}\frac{\partial p_n'}{\partial y}+\frac{1}{h}\frac{\partial}{\partial x}\left(\bar{\nu}_t h\frac{\partial \bar{v}}{\partial x}\right)+\frac{1}{h}\frac{\partial}{\partial y}\left(\bar{\nu}_t h\frac{\partial \bar{v}}{\partial y}\right)$$
$$-\frac{C_\tau \bar{\nu}_t}{h^2}\bar{v}+\frac{F_y}{\rho h}+\frac{W_y}{\rho h} \tag{36}$$

and the depth-averaged equation of continuity:

$$\frac{\partial h}{\partial t}+\frac{\partial(\bar{u}h)}{\partial x}+\frac{\partial(\bar{v}h)}{\partial y}=0 \tag{37}$$

it forms the well-known shallow-water equations. Program packages, solving these equations on a routine basis, are amply available by now. The non-linearity of the bottom shear stress term, due to the fact that C_τ and $\bar{\nu}_t$ depend on $\bar{u}_{tot}$, can be dealt with in the usual way, by iteration or by estimation from the results for the preceding time step. As was stated before, the usual formulation of the wave-induced forces on the basis of the radiation stress gradients:

$$F_x=-\frac{\partial S_{xx}}{\partial x}-\frac{\partial S_{xy}}{\partial y} \quad \text{and} \quad F_y=-\frac{\partial S_{xy}}{\partial x}-\frac{\partial S_{yy}}{\partial y} \tag{38}$$

is formally correct, but it can give rise to spurious numerical effects (De Vriend, 1985b; Dingemans et al., 1987). These are mainly caused by the part of the force field that, divided by ρh, is irrotational and hence unable to drive a net current (Battjes, 1974). If the water surface elevation induced by this irrotational part of $\boldsymbol{F}/\rho h$ (e.g. the set-down in the wave shoaling area at a uniform beach) is small compared with the water depth, it is preferable to retain only the irrotational part. The corresponding part of the force can be written as (Longuet-Higgins, 1970; Dingemans et al., 1987):

$$F_x'=\frac{D}{c_w}\cos\theta \quad \text{and} \quad F_y'=\frac{D}{c_w}\sin\theta \tag{39}$$

in which c_w is the phase-celerity of the waves and θ is the direction of the energy flux, with reference to the x-axis. So the part of the force that is able to drive a net current is proportional to the energy dissipation rate per unit area, D, and has the same direction as the wave energy flux.

WAVE-INDUCED SECONDARY CURRENT

Three-layer concept

In order to describe the wave-induced secondary current, the water column is divided into three layers:
- a surface layer, above the wave trough level;

– a middle layer; and
– a bottom layer.

The surface layer contains the moving water surface, which makes a continuum description of the water motion here particularly difficult. On the other hand, this description, itself, is not of primary interest to the present model, if only the effects of the top layer on the layers below can be identified. Svendsen (1985) and Stive and Wind (1986) propose to consider only the area below the wave trough level, and to take account of the surface layer effects via an effective shear stress at the trough level, compensating for the momentum decay above it, and via the condition that the net undertow must compensate for the mass flux in the surface layer. This means that the surface layer model is reduced to the formulation of the effective shear stress and the mass flux.

The rationale followed to derive the secondary flow equation (23) from the general x-momentum equation (18) can also be applied to the area below the wave trough level. Considering wave-induced currents only, this leads to the following x-momentum equation for the middle layer:

$$\frac{\partial}{\partial z}\left(\nu_t \frac{\partial u_s}{\partial z}\right) - \frac{\tau_{tsx} - \tau_{bsx}}{\rho(z_t - z_b)} + f_c(v_s - \bar{v}_{s,r}) = \frac{\partial}{\partial x}(\langle \tilde{u}^2 \rangle - \langle \tilde{w}^2 \rangle)$$

$$-\frac{1}{z_t - z_b}\int_{z_b}^{z_t} \frac{\partial}{\partial x}(\langle \tilde{u}^2 \rangle - \langle \tilde{w}^2 \rangle)\,dz + \frac{\partial}{\partial y}(\langle \tilde{u}\tilde{v} \rangle) - \frac{1}{z_t - z_b}\int_{z_b}^{z_t} \frac{\partial}{\partial y}(\langle \tilde{u}\tilde{v} \rangle)\,dz \quad (40)$$

in which τ_{ts} denotes the effective shear stress at the wave trough level z_t and $\bar{v}_{s,r}$ is the y-velocity component of the mean return current (undertow). In the case of an irrotational wave field on a horizontal bottom, the right-hand part of this equation is identically equal to zero. In a practical situation, with random waves, breaking and non-breaking, in combination with a turbulent net current on an uneven bottom topography, this is not exactly the case. Still the right-hand part of eqn. (40) is assumed to be negligibly small for the non-breaking fraction of the waves (also see Craik, 1982).

Stive and Wind (1986) show that the effective stress terms in eqn. (40), as far as they are due to breaking waves, are hardly varying with z. This means, that for the breaking fraction of the waves the right-hand part of eqn. (40) is also virtually equal to zero.

The coriolis-terms in eqn. (40) and its y-equivalent are usually small compared with the other terms. Their principal effect is a tendency of the velocity vector to rotate with z (Ekman, 1905). In general, this effect is negligible if (e.g. see Neuman and Pierson, 1966):

$$h \ll \left(\frac{2\bar{\nu}_t}{f_c}\right)^{1/2} \quad (41)$$

Especially in the relatively shallow breaker zone, this will mostly be the case. Then the reduced version of the equation becomes:

$$\frac{\partial}{\partial z}\left(\nu_t \frac{\partial u_s}{\partial z}\right)=\frac{\tau_{tsx}-\tau_{bsx}}{\rho(z_t-z_b)} \tag{42}$$

Without giving an exact proof, the shear stresses at the wave trough level and at the bottom, as well as the mass flux in the surface layer, are assumed to have the same direction as the wave-energy flux. As a consequence, the wave-induced secondary current described by eqn. (42) will also have the direction of the energy flux. So:

$$u_s = U_s(x,y;\zeta)\cos\theta \quad \text{and} \quad v_s = U_s(x,y;\zeta)\sin\theta \tag{43}$$

The velocity in the bottom layer, where the sediment concentrations are usually highest, can contribute substantially to the total sediment transport. Because of the natural irregularity of a mobile bottom, however, a detailed description of this velocity hardly makes sense, unless it is needed to assess the influence on the velocity in the middle layer. Therefore, the bottom layer velocity due to non-breaking waves is assumed to be similar to Longuet-Higgins' (1953) "conduction solution" for progressive waves (also see Phillips, 1977 and Craik, 1982). For breaking waves, Stive and Wind (1986) show that assuming a zero bottom shear stress leads to acceptable predictions of the secondary current outside the wave boundary layer. This means that for this part of the current the bottom layer as such can be left out of consideration. Thus the problem has been reduced to solving the velocity in the middle layer from eqn. (42), both for the breaking and the non-breaking fraction of the waves. In either cases the prescribed shear stress at the wave trough level provides an upper boundary condition, whereas the lower boundary condition follows from the zero shear stress approximation (breaking waves) or from matching with the bottom layer solution (non-breaking waves). The integral condition of continuity can be used to determine the remaining unknown constant (the bottom shear stress for non-breaking waves, the mean return current velocity for breaking waves). In the next sections these middle-layer solutions will be considered in further detail, for non-breaking waves, for breaking waves and for a random wave field with a fraction of breaking waves, respectively.

Secondary current induced by non-breaking waves

The secondary current model for the non-breaking part of the waves is very much like Longuet-Higgins' (1953) conduction solution for progressive waves, as reformulated by Phillips (1977) and Craik (1982).

If there is no mean pressure gradient, the velocity in the bottom layer is given by:

$$U_{nb_1}=\frac{\bar{U}_{orb}^2}{4c_w}\left[3-\{2(2+Z)\cos Z-2(1-Z)\sin Z-\exp(-Z)\}\exp(-Z)\right] \quad (44)$$

in which $\bar{U}_{orb}$ is the amplitude of the near-bottom orbital velocity and Z is the vertical co-ordinate, scaled by the thickness δ of the wave boundary layer.

In the present case, the mean pressure gradient cannot be disregarded beforehand, which means that there is an additional component of the bottom layer velocity, described by:

$$\frac{\partial}{\partial z}\left(\nu_t\frac{\partial U_{nb_2}}{\partial z}\right)=\text{constant} \quad (45)$$

This equation is not essentially different from eqn. (22) and the resulting velocity distribution will be similar to the near-bottom distribution of the primary flow. This means that the logarithmic part ($\ln\zeta$) of the secondary velocity in the middle-layer has its point of zero intersection at $\zeta=F'\zeta_o$ and that the corresponding bottom-layer velocity distribution is linear between $\zeta=0$ and $\zeta=F\zeta_o$ (Nielsen, 1985).

According to Longuet-Higgins' theory, there is a weak viscous boundary layer near the liquid surface, responsible for a mean velocity outside this layer:

$$\frac{\partial U_{nb}}{\partial z}=\frac{\bar{U}_{orb}^2 k_w}{c_w}\sinh(2k_w h) \quad (46)$$

Although the present case is not exactly the same as the one considered by Longuet-Higgins, this vorticity is assumed to be present at the wave trough level, where it is imposed as a boundary condition to the velocity in the middle layer. In terms of the shear stress, this condition reads:

$$\tau_{ts}^{(nb)}=\rho\nu_t|_{z_t}\frac{\bar{U}_{orb}^2 k_w}{c_w}\sinh(2k_w h)=4\nu_t|_{z_t}\frac{k_w^2 E_{nb}}{c_w} \quad (47)$$

in which E_{nb} denotes the energy density of the non-breaking wave field.

In the absence of a mean pressure gradient, the bottom boundary condition for the middle-layer velocity would follow from matching with the bottom-layer solutions (44):

$$U_{nb}|_{z_b}=\frac{3}{4}\frac{\bar{U}_{orb}^2}{c_w} \quad (48)$$

In the presence of a mean pressure gradient, a compound bottom boundary condition is imposed: a prescribed level of zero intersection $F'\zeta_o$ (see eqn. (25) sqq.) for the logarithmic part ($\ln\zeta$) of U_{nb} and condition (48) for the remainder.

The integral condition of continuity implies that the mass flux in the surface layer is compensated by a return current in the lower layers. For non-breaking progressive waves, this mass flux follows from (Phillips, 1977):

$$m_{nb} = \frac{E_{nb}}{c_w} \tag{49}$$

whence

$$\int_{z_b}^{z_t} U_{nb}\,dz = -\frac{E_{nb}}{\rho c_w} \tag{50}$$

The contribution of the bottom layer velocity U_{nb_1} to the integral amounts:

$$\int_{z_b}^{z_t} U_{nb_1}\,dz = \delta \int_0^{\infty} U_{nb_1}\,dZ = \frac{3}{8}\delta \frac{\bar{U}_{orb}^2}{c_w} = \frac{3}{2} \frac{k_w \delta}{\sinh(2k_w h)} \frac{E_{nb}}{\rho c_w} \tag{51}$$

which is negligible as $\delta \ll h$. This means that eqn. (50) applies to the middle layer solution only.

The velocity in the middle layer, except for the constant τ_{bs}, can be solved from eqn. (42) and two out of the three conditions (47), (49) and (50). The constant τ_{bs} follows from the remaining condition. More or less arbitrarily, the combination of eqns. (42) and (47) and the compound bottom boundary condition is chosen to solve for U_{nb}. Then condition (50) remains to determine τ_{bs}.

For the turbulence viscosity model defined before, the solution in the middle layer can be written into the form of the similarity series (7), to yield:

$$U_{nb} = \bar{U}_{nb_1} f_{s_1}(\zeta) + \bar{U}_{nb_2} f_{s_2}(\zeta) + \bar{U}_{nb_3} \tag{52}$$

in which

$$\bar{U}_{nb_1} = \frac{\tau_{ts}^{(nb)} h}{\rho \bar{\nu}_t \zeta_t} \quad ; \quad \bar{U}_{nb_2} = \frac{\tau_{bs}^{(nb)} h}{\rho \bar{\nu}_t \zeta_t} \quad ; \quad \bar{U}_{nb_3} = \frac{3}{4} \frac{\bar{U}_{orb}^2}{c_w} \tag{53}$$

and

$$\frac{\partial}{\partial \zeta}\left(\phi \frac{\partial f_{s_1}}{\partial \zeta}\right) = 1 \quad \text{with} \quad \left(\phi \frac{\partial f_{s_1}}{\partial \zeta}\right)\Big|_{\zeta_t} = \zeta_t \quad \text{and} \quad f_{s_1}(0) = 0 \tag{54}$$

$$\frac{\partial}{\partial \zeta}\left(\phi \frac{\partial f_{s_2}}{\partial \zeta}\right) = -1 \quad \text{with} \quad \left(\phi \frac{\partial f_{s_2}}{\partial \zeta}\right)\Big|_{0} = \zeta_t \quad \text{and} \quad f_{s_2}(F'\zeta_o) = 0 \tag{55}$$

For the compound ϕ-distribution (17), the solutions of the systems (54) and (55) read:

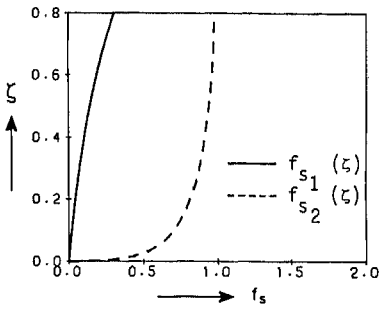

Fig. 4. Vertical distribution functions for the wave-induced secondary flow (conditions TOW-campaign Dec., 1982 at Egmond beach, location $x=200$ m; see Table 3).

$$f_{s_1} = \begin{cases} -\frac{5}{24}\ln(1-\zeta) & \text{for } \zeta \leqslant \frac{1}{2} \\ \frac{5}{12}\zeta^2 + \frac{5}{48}(2\ln 2 - 1) & \text{for } \zeta \geqslant \frac{1}{2} \end{cases} \tag{56}$$

$$f_{s_2} = \begin{cases} \frac{5}{24}\zeta_t[\ln\zeta - \ln(F'\zeta_o)] + \frac{5}{24}(1-\zeta_t)\ln(1-\zeta) & \text{for } F\zeta_o \leqslant \zeta \leqslant \frac{1}{2} \\ \frac{5}{12}(2\zeta_t\zeta - \zeta^2) - \frac{5}{24}\zeta_t[2+\ln(F'\zeta_o)] - \frac{5}{48}(2\ln 2 - 1) & \text{for } \zeta \geqslant \frac{1}{2} \end{cases} \tag{57}$$

The vertical distribution functions $f_{s_1}(\zeta)$ and $f_{s_2}(\zeta)$ are shown in Fig. 4. Making use of eqns. (56) and (57), the integral condition of continuity (50) can be elaborated to:

$$C_1 \bar{U}_{nb_1} + C_2 \bar{U}_{nb_2} + \bar{U}_{nb_3} = -\frac{E_{nb}}{\rho c_w h \zeta_t} \tag{58}$$

in which:

$$C_1 = \frac{5}{36}\zeta_t^2 + \frac{5}{48}(2\ln 2 - 1) - \frac{5}{72}\frac{1}{\zeta_t}(3\ln 2 - 2) \tag{59}$$

$$C_2 = \frac{5}{18}\zeta_t^2 - \frac{5}{12}\zeta_t - \frac{5}{24}(2\ln 2 - 1) + \frac{5}{72}\frac{1}{\zeta_t}(3\ln 2 - 2) - \frac{5}{24}\zeta_t \ln(F'\zeta_o) \tag{60}$$

Combined with the bottom layer solution, expression (52) can be elaborated to:

$$U_{nb} = \bar{U}_{nb_1}\left\{f_{s_1}(\zeta) - \frac{C_1}{C_2}f_{s_2}(\zeta)\right\} + \bar{U}_{nb_3}\left\{1 - \frac{1}{C_2}f_{s_2}(\zeta)\right\} + \bar{U}_{nb_3}f_{s_b}(\zeta) - \frac{E_{nb}}{\rho c_w h \zeta_t}\frac{1}{C_2}f_{s_2}(\zeta) \tag{61}$$

in which, according to eqn. (44):

$$f_{sb}(\zeta)=\exp\left(-\frac{h\zeta}{\delta}\right)\left[\exp\left(-\frac{h\zeta}{\delta}\right)+2\left(1-\frac{h\zeta}{\delta}\right)\sin\left(\frac{h\zeta}{\delta}\right)-2\left(2+\frac{h\zeta}{\delta}\right)\cos\left(\frac{h\zeta}{\delta}\right)\right] \tag{62}$$

and (cf. Nielsen, 1985):

$$f_{s2}(\zeta)=\frac{5}{24}\zeta_t\left(1-\frac{1}{F}\right)\frac{\zeta}{F\zeta_o} \quad \text{for} \quad \zeta\leqslant F\zeta_o \tag{63}$$

In order to have an indication of the relative importance of the various constituents in eqn. (61), U_{nb} is elaborated for two sets of parameters (see Table 1), corresponding with the conditions during one of the NSTS-experiments at Torrey Pines Beach, San Diego, California on Nov. 20, 1978 (Guza and Thornton, 1985) and with those during one of the TOW-experiments at Egmond, The Netherlands (Derks and Stive, 1984), viz. case 18 documented in Battjes and Stive (1985).

Inspection of Fig. 5 indicates that the secondary current is dominated by the second and the fourth term of eqn. (61). The former expresses the effect of the bottom shear stress arising from the oscillatory wave boundary layer, while the latter compensates for the mass flux above wave trough level. With reference to the discussions of Figs. 7 and Fig. 8 further on, it is concluded that the current velocities are relatively weak (note that the same scales are used throughout Figs. 5, 7 and 8).

It has to be noted that under these conditions, where the coriolis-effect is certainly not negligible, the actual velocity distributions can be quite different from those presented herein (e.g. see Jenkins, 1987). Nevertheless, the latter give an indication of the overall order of magnitude of the velocities and the relative importance of their driving mechanisms. Besides, as soon as there is a net current (e.g. tidal) superimposed, $\bar{\nu}_t$ will rise by orders of magnitude and the coriolis-effect becomes much less important.

TABLE 1

Parameters for sample computations of U_{rb}

	X (m)	h (m)	H_{rms} (m)	T_p (s)	$\bar{U}_{orb}$ (m/s)	$\tilde{\nu}_t$ (m²/s)	$\left(\frac{2\tilde{\nu}_t}{f_c h^2}\right)^{\frac{1}{2}}$
T. Pines	350	5.19	0.61	14.3	0.41	1.0×10^{-6}	0.03
Egmond	2000	16.15	2.78	8.7	0.77	1.0×10^{-6}	0.01

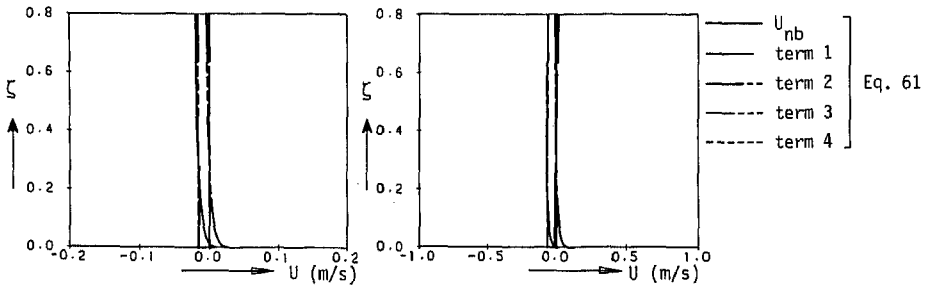

Fig. 5. Constituents contributing to the wave-induced secondary flow below wave trough level; conditions non-breaking waves (see Table 1) at Torrey Pines beach, NSTS-campaign Nov. 20, 1978 (left) and at Egmond beach, TOW-campaign Dec., 1982 (right).

Secondary current induced by breaking waves

The concept of the secondary current model for the breaking part of the waves is the same as proposed by Stive and Wind (1986), but the elaboration is somewhat different.

The shear stress at the bottom is taken equal to zero, which the same authors show to yield quite acceptable secondary current velocities. The shear stress at the wave trough level is described by the expression given by Stive and Wind on the basis of earlier work by Svendsen (1984 and 1985):

$$\tau_{ts}^{(br)} = \left(\frac{1}{2} + 7\frac{h}{\lambda}\right)\frac{D}{c_w} \tag{64}$$

in which λ is the wave length at breaking. The second part of the factor in brackets accounts for the contribution of the surface roller. Apart from the factor in brackets, this expression shows a strong resemblance with expression (39) for the wave-induced driving force. This is not surprising, as they are both related to the same phenomenon: the momentum decay due to breaking.

The mass flux above the wave trough level is assumed to consist of two parts, one due to the progressive character of the breaking waves [also see eqn. (49)] and the other one due to the surface roller (Svendsen, 1984). This leads to:

$$m_{br} = \left(1 + 7\frac{h}{\lambda}\right)\frac{E_{br}}{c_w} \tag{65}$$

Note the resemblance of the roller contributions in expressions (64) and (65). This is a direct consequence of Svendsen's approach of the water motion in the surface layer.

The velocity in the middle layer follows from eqn. (42) with $\tau_{bs}^{(bs)} = 0$, the shear stress condition (64) and the integral condition of continuity based on eqn. (65). For the adopted turbulence viscosity model, the solution can be written into the form:

$$U_{\mathrm{br}} = \bar{U}_{\mathrm{br}_1}[f_{s_1}(\zeta) - C_1] + \bar{U}_{\mathrm{br}_3} \tag{66}$$

in which

$$\bar{U}_{\mathrm{br}_1} = \frac{\tau_{ts}^{(\mathrm{br})} h}{\rho \bar{\nu}_t \zeta_t} \quad ; \quad \bar{U}_{\mathrm{br}_3} = -\frac{m_{\mathrm{br}}}{\rho h \zeta_t} \tag{67}$$

and the vertical distribution function $f_{s_1}(\zeta)$ is identical to the one for non-breaking waves, given by expression (56).

Figure 6 shows the resulting wave-induced currents for a laboratory experiment with regular breaking waves (Buhr-Hansen and Svendsen, 1984), together with the corresponding model results for a constant eddy viscosity (Stive and Wind, 1986). The two computed distributions turn out to be very similar and they agree well with the measured data. So, also in this respect the present model corresponds well with a verified specific model.

In order to estimate the relative importance of the constituents in eqn. (66), U_{br} is elaborated for two sets of parameters (see Table 2), again from Torrey Pines Beach and from Egmond.

Figure 7 shows, that the second term of eqn. (66) is mainly responsible for the depth-averaged net value of the secondary current and that the first term is responsible for its vertical variation. The first term expresses the effect of the shear stress at trough level arising from the wave momentum loss, while the second term compensates for the mass flux above wave trough level. The current velocities are relatively strong.

The present formulation is claimed to predict the breaking-induced secondary current velocity outside the bottom boundary layer. It provides no reliable information on the velocity inside this layer, nor on the attending bottom shear stress. Hence, a composition of the primary and secondary bottom shear stress makes no sense in this model and caution should be exercised when evaluating the magnitude and the direction of the sediment transport on the basis of these results. From this point of view, the model needs further improvement, requiring a more detailed investigation of the bottom layer current under breaking waves (see Svendsen, 1985; Schäffer and Svendsen, 1986; Stive and De Vriend, 1987).

Secondary current in a random surf zone

In a surf zone with random waves, only part of the waves are breaking, say a fraction $\tilde{Q}_b$ ($0 \leqslant \tilde{Q}_b \leqslant 1$). If mutual interaction between the waves is left out of consideration, this means that the secondary current velocities for the breaking and the non-breaking waves have to be added with appropriate weight factors.

Combining eqns. (52) and (66) in this way yields:

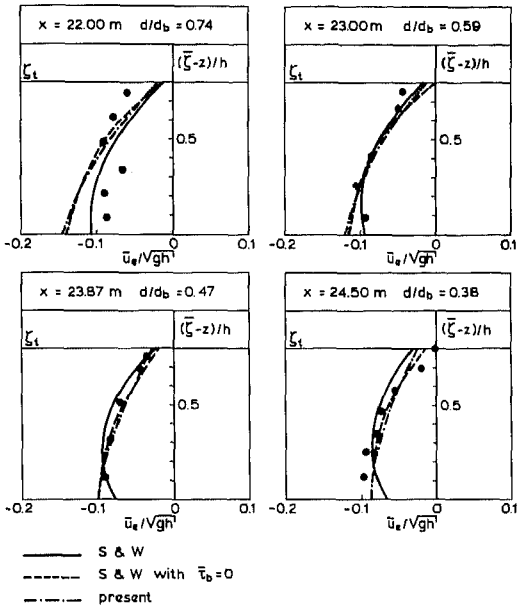

Fig. 6. Wave-induced secondary flow: comparison between measurements and theory for a monochromatic wave train on a constant slope (measurements after Buhr-Hansen and Svendsen, 1984). Data points: measured values. Curves: computations with the several models, see legend; *S & W* is Stive and Wind (1986), *S & W* with $\tau(b)=0$ is Stive and Wind (1986) with bottom shear stress neglected, and *present* is present model.

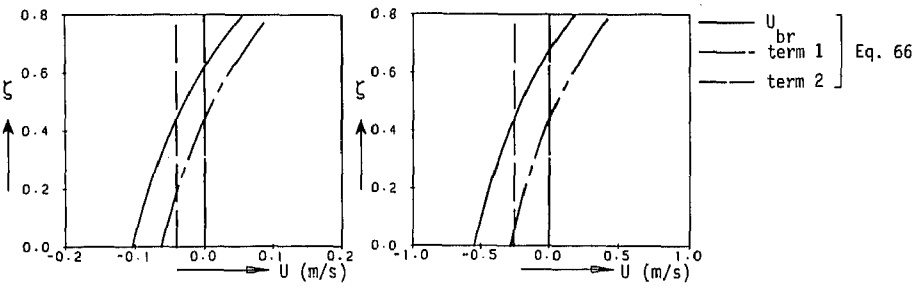

Fig. 7. For legend, see Fig. 5; conditions full breaking waves (see Table 2).

TABLE 2

Parameters for sample computations of U_{br}

	X (m)	h (m)	H_{rms} (m)	T_p (s)	$\tilde{Q}_b$ (-)	D (N/ms)	$\tilde{\nu}_t$ (m²/s)	$\left(\frac{2\tilde{\nu}_t}{f_c h^2}\right)^{\frac{1}{2}}$
T. Pines	105	0.33	0.12	14.3	1.00	5.5	1.5×10^{-3}	18.2
Egmond	50	1.60	0.89	8.7	1.00	104.1	1.9×10^{-2}	11.2

$$U_{rb} = \bar{U}_{rb_{1a}}[f_{s_1}(\zeta) - C_1] + \bar{U}_{rb_{1b}}[f_{s_1}(\zeta) - C_1] + \bar{U}_{rb_2}[f_{s_2}(\zeta) - C_2] + \bar{U}_{rb_{3a}} + \bar{U}_{rb_{3b}} + \bar{U}_{rb_4} f_{s_b}(\zeta) \tag{68}$$

in which $f_{s_1}(\zeta)$, $f_{s_2}(\zeta)$, $f_{s_b}(\zeta)$, C_1 and C_2 are given by expressions (56), (57), (63), (59) and (60), respectively. After some elaboration, the quantities $\bar{U}_{rb_1}$, $\bar{U}_{rb_2}$, $\bar{U}_{rb_3}$ and $\bar{U}_{rb_4}$ can be written as:

$$\bar{U}_{rb_{1a}} = (1 - \tilde{Q}_b)\frac{24}{5}\frac{k_w^2 hE}{\rho c_w \zeta_t} \tag{69a}$$

$$\bar{U}_{rb_{1b}} = \left(\frac{1}{2} + 7\frac{h}{\lambda}\right)\frac{hD}{\rho c_w \bar{\nu}_t \zeta_t} \tag{69b}$$

$$\bar{U}_{rb_2} = -\frac{1 - \tilde{Q}_b}{C_2}\left[\frac{3}{4}\frac{\bar{U}_{orb}^2}{c_w} + \left(1 + \frac{24}{5}k_w^2 h^2 C_1\right)\frac{E}{\rho c_w h \zeta_t}\right] \tag{70}$$

$$\bar{U}_{rb_{3a}} = -(1 - \tilde{Q}_b)\frac{E}{\rho c_w h \zeta_t} \tag{71a}$$

$$\bar{U}_{rb_{3b}} = -\tilde{Q}_b\left(1 + 7\frac{h}{\lambda}\right)\frac{E}{\rho c_w h \zeta_t} \tag{71b}$$

$$\bar{U}_{rb_4} = (1 - \tilde{Q}_b)\frac{3}{4}\frac{\bar{U}_{orb}^2}{c_w} \tag{72}$$

in which E denotes the energy density of the total wave field.

The relative importance of the various constituents of U_{rb} is estimated, once again, for parameter sets from the experiments at Torrey Pines Beach and at Egmond (see Table 3).

Detailed inspection of Fig. 8 shows that in the random breaking situation the effects expressed by terms 2...5 of eqn. (68) contribute to the secondary current. The terms 2 and 5 are due to the breaking wave fraction and comparable to the terms 1 and 2 of eqn. (66). The terms 3 and 4 are due to the non-breaking wave fraction and comparable to the terms 2 and 4 of eqn. (61). The

TABLE 3

Parameters for sample computation of U_{rb}

	x (m)	h (m)	H_{rms} (m)	T_p (s)	$\tilde{Q}_b$ (-)	D (N/ms)	$\tilde{\nu}_t$ (m²/s)	$\left(\frac{2\tilde{\nu}_t}{f_c h^2}\right)^{\frac{1}{2}}$
T. Pines	190	1.51	0.44	14.3	0.43	28.8	1.1×10^{-2}	10.8
Egmond	200	4.13	1.68	8.7	0.32	116.4	5.1×10^{-2}	7.1

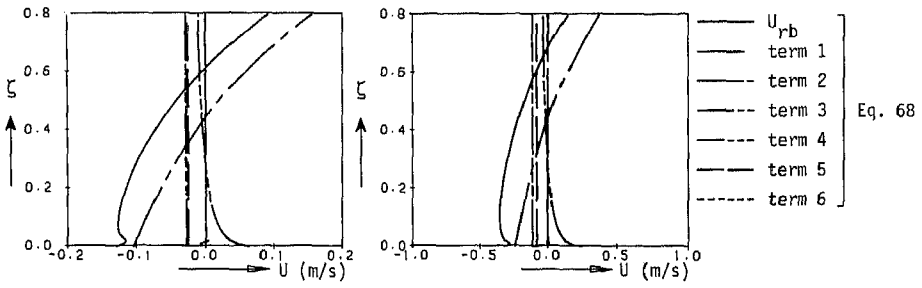

Fig. 8. For legend, see Fig. 5; conditions random breaking waves (see Table 3).

relatively high secondary current velocities are nearly equally due to the breaking and the non-breaking waves.

A comparison with the measured data from Torrey Pines Beach is given in Fig. 9. The wave energy decay prediction [Battjes and Stive (1985) model, $x=5.0$ and $\gamma=0.5$] was calibrated on the basis of the measured orbital velocity variance in the frequency range $0.05<f<0.5$ Hz. The velocity measurements were conducted at elevations of 0.4 m to 1.0 m above the bed. Taking account of the inherent inaccuracy of the measured, wave-induced cross-shore velocities, the agreement is good, for the magnitude of the velocity as well as for its cross-shore distribution of the velocity. For the purpose of comparison also the prediction for the Egmond Beach is given. The wave energy decay prediction is according to the method proposed by Battjes and Stive (1985). It is noted that the storm conditions in this case generate strong secondary currents.

RELATIVE IMPORTANCE OF WAVE-INDUCED SECONDARY CURRENTS

Cross-shore sediment transport

The importance of the wave-induced secondary current is difficult to judge from its magnitude alone, especially from a morphological point of view. A comparison with the longshore current velocity is elucidating, as will be shown hereafter, but it provides insufficient information on the morphological impact of the secondary flow. In this respect, a better picture can probably be obtained by comparing the cross-shore sediment transport rate due to this current with the transport rates due to other mechanisms acting in the cross-shore plane (wave asymmetry, bottom slope).

This idea can be worked out on the basis of the sediment transport formulation proposed by Bailard (1982), which was elaborated and applied in practice by Stive (1985, 1986):

$$\langle i_x \rangle = B_b\{\langle |u|^2 u\rangle - \frac{\langle |u|^3\rangle}{\tan\psi}\frac{\partial z_b}{\partial x}\} + B_s\{\langle |u|^3 u\rangle - \frac{\epsilon_s}{W}\langle |u|^5\rangle \frac{\partial z_b}{\partial y}\}$$

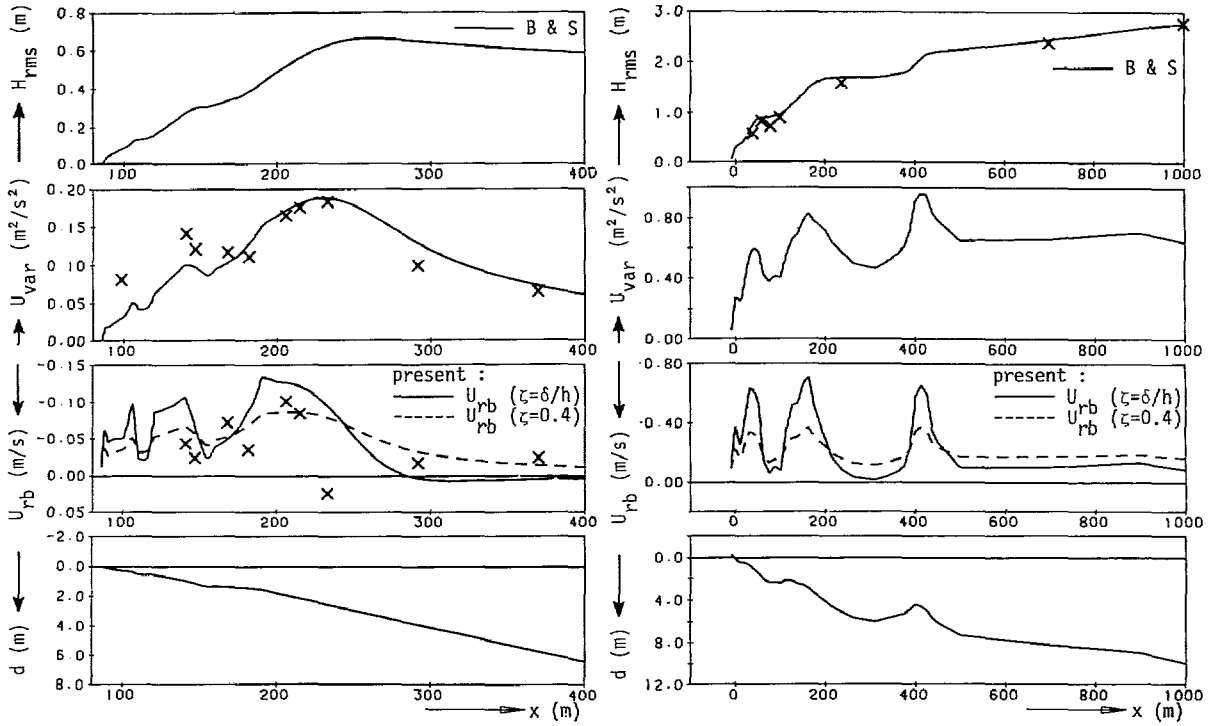

Fig. 9. results for NSTS-campaign Nov. 20, 1978 at Torrey Pines beach (measurements after Guza and Thornton, 1985) (left) and for TOW-campaign Dec., 1982 at Egmond (measurements after Derks and Stive, 1984) (right); profiles of bottom elevation below MSL (d), cross-shore current (U_{rb}), variance of horizontal orbital velocity (U_{var}), and rms wave height (H_{rms}) versus distance normal to shore (x). Data points: measured values. Curves: computations with the models, see legend; *B & S* is Battjes and Stive (1985), *present* is present model, where U_{rb} ($\zeta=\delta/h$) is the secondary flow on top of the bottom boundary layer and U_{rb} ($\zeta=0.4$) is that at 0.4 times the water depth.

in which
i_x = instantaneous cross-shore sediment transport rate,
B_b = constant for the bed-load part of the transport,
u = instantaneous near-bottom velocity,
ψ = internal angle of friction of the sediment,
B_s = constant for the suspended-load part of the transport,
ϵ_s = a constant (usually taken 0.02), and
W = fall velocity of the sediment.
Assuming the near-bottom current velocity to be small compared with the wave orbital velocity near the bottom and estimating the odd moments of the orbital velocity on the basis of second-order Stokes theory with a locked but non-zero phase lag ϕ_2 between the two components, Stive (1985, 1986) elaborates this formula to:

$$\langle i_x \rangle = \langle i_{asb} \rangle + \langle i_{ass} \rangle + \langle i_{ncb} \rangle + \langle i_{ncs} \rangle - \langle i_{slb} \rangle - \langle i_{sls} \rangle \tag{74}$$

in which

$$\langle i_{asb} \rangle = \frac{9}{16} B_b \frac{\bar{U}_{orb}^4}{c_w \sinh^2 (k_w h)} \cos\phi_2; \quad \langle i_{ass} \rangle = \frac{9}{5\pi} B_s \frac{\bar{U}_{orb}^5}{c_w \sinh^2 (k_w h)} \cos\phi_2 \tag{75}$$

$$\langle i_{ncb} \rangle = \frac{3}{2} B_b \bar{U}_{orb}^2 \langle u \rangle \; ; \qquad \langle i_{ncs} \rangle = 6.4 B_s \bar{U}_{orb}^3 \langle u \rangle \tag{76}$$

$$\langle i_{slb} \rangle = 1.6 \frac{B_b}{\tan\psi} \bar{U}_{orb}^3 \frac{\partial z_b}{\partial x} \; ; \qquad \langle i_{sls} \rangle = 8 \frac{\epsilon_s B_s}{W} \bar{U}_{orb}^5 \frac{\partial z_b}{\partial x} \tag{77}$$

Making use of these results, effective transport velocities can be defined for the bed-load and suspended-load parts of the transport components due to wave asymmetry and bottom slope effects:

$$U_{asb} = \frac{\langle i_{asb} \rangle}{\langle i_{ncb} \rangle} \langle u \rangle = \frac{3}{8} \frac{\bar{U}_{orb}^2}{c_w \sinh^2 (k_w h)} \cos\phi_2 \tag{78}$$

$$U_{ass} = \frac{\langle i_{ass} \rangle}{\langle i_{ncs} \rangle} \langle u \rangle = \frac{9}{32\pi} \frac{\bar{U}_{orb}^2}{c_w \sinh^2 (k_w h)} \cos\phi_2 \tag{79}$$

$$U_{slb} = \frac{\langle i_{slb} \rangle}{i_{ncb} \rangle} \langle u \rangle = 1.1 \frac{\bar{U}_{orb}}{\tan\phi} \left| \frac{\partial z_b}{\partial x} \right| \tag{80}$$

$$U_{sls} = \frac{\langle i_{sls} \rangle}{\langle i_{ncs} \rangle} \langle u \rangle = 1.2 \frac{\epsilon_s}{W} \bar{U}_{orb}^2 \left| \frac{\partial z_b}{\partial x} \right| \tag{81}$$

These effective transport velocities provide a reference for the near-bottom secondary current velocity. As an example, they are elaborated for the two

sections at Torrey Pines Beach and Egmond, with $\tan\phi=0.6$, $\epsilon_s=0.02$, $W=0.28$ and assuming $\cos\phi_2=1-\tilde{Q}_b$. Furthermore, $\bar{U}_{orb}$ is related to the orbital velocity variance as $\bar{U}_{orb}=(2U_{var})^{\frac{1}{2}}$, such that a monochromatic wave field of velocity amplitude $\bar{U}_{orb}$ has the same variance as the random wave field. The results are shown in Fig. 10, together with the near-bottom values of $(1-\tilde{Q}_b)\ U_{nb}$ and $\tilde{Q}_b U_{br}$. Apparently, there are two important contributions to the sediment transport, represented by the wave-induced secondary current and the asymmetry-induced effective current in the bottom layer. In low-frequency or swell conditions (Torrey Pines) the latter dominates and in high-frequency or storm conditions (Egmond) the former dominates. These conclusions coincide with the common suggestion that low-frequency waves build up a coast and that high-frequency waves erode it.

Combined nearshore current velocity

The importance of the wave-induced secondary flow for the nearshore current field can be estimated by comparing it with the wave-induced longshore current along a uniform beach. The depth-averaged longshore current velocity in such a situation can be derived from eqns. (28) and (39), to yield:

$$\bar{v}=\frac{1}{C_\tau}\frac{Dh}{\rho c_w \bar{\nu}_t}\sin\theta \tag{82}$$

The near-bottom secondary velocity in the saturated surf zone is entirely dominated by the breaking-induced undertow, described by eqn. (66). For convenience, only the near-bottom velocity due to the effective shear stress $\tau_{ts}^{(br)}$ is considered, which implies a conservative estimate:

$$U_{br}\approx-\left(\tfrac{1}{2}+7\frac{h}{\lambda}\right)\frac{Dh}{\rho c_w \bar{\nu}_t}\frac{C_1}{\zeta_t} \tag{83}$$

with 0.15 as a typical value of the last factor (it is noted that $\zeta_t\approx 0.8$ has been used as an estimate throughout).

In the present model, the vertical variation of the primary velocity is described by $f_p(\zeta)$, which goes to zero at the bottom, whereas U_{br} has a finite value there. Hence a comparison of the velocities at the bottom makes no sense. Moreover, the model gives a very strong vertical variation of the ratio of cross-shore and longshore velocities near the bottom, so that selecting another near-bottom level for such a comparison is difficult, as well. Therefore, a pragmatic approach is chosen, with 0.5 $\bar{v}$ as a representative value of the near-bottom primary velocity.

As $\boldsymbol{U}_{br}$ has the direction of the wave energy flux, its composition with 0.5 $\bar{v}$ yields:

$$|u_{tot}|=\{\langle 0.5\,\bar{v}+U_{br}\sin\theta)^2+U_{br}^2\cos^2\theta\}^{1/2} \tag{84}$$

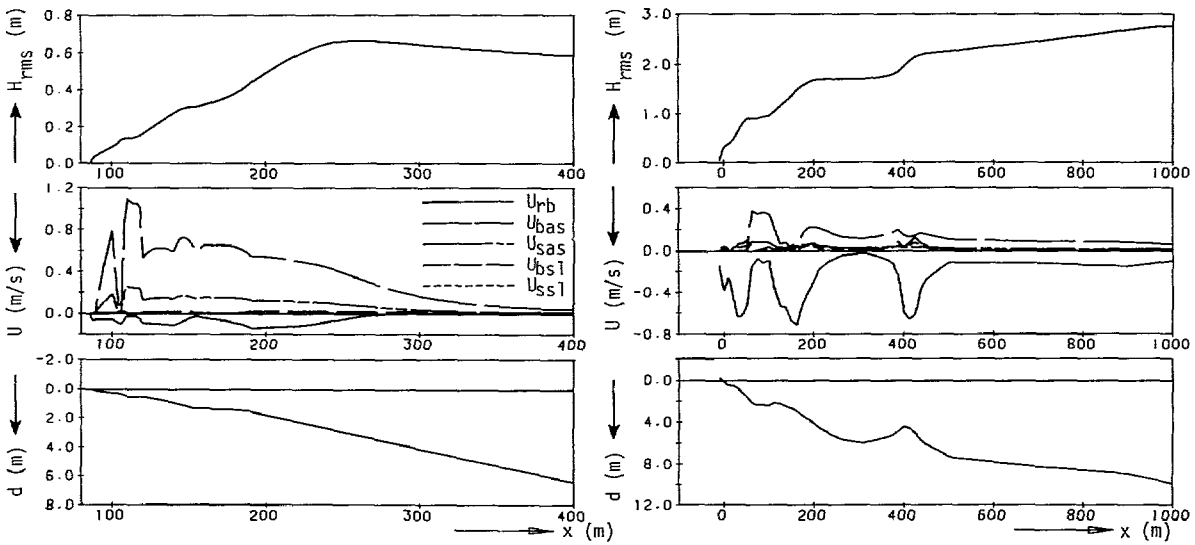

Fig. 10. Comparison between the effective transport velocities and the near-bottom secondary current velocity; conditions at Torrey Pines beach, NSTS-campaign Nov. 20, 1978 (left) and at Egmond beach, TOW-campaign Dec., 1982 (right).

$$=\frac{Dh}{\rho c_w \bar{v}_t}\left[\left\{0.25\,C_\tau^{-2}-0.15\,C_\tau^{-1}\left(\tfrac{1}{2}+7\frac{h}{\lambda}\right)\right\}\sin^2\theta+0.023\left(\tfrac{1}{2}+7\frac{h}{\lambda}\right)^2\right]^{1/2} \quad (85)$$

$$\tan\alpha=\frac{0.5\,\bar{v}+U_{br}\sin\theta}{U_{br}\cos\theta}=\frac{0.5\,C_\tau^{-1}-0.15\left(\tfrac{1}{2}+7\frac{h}{\lambda}\right)}{-0.15\left(\tfrac{1}{2}+7\frac{h}{\lambda}\right)}\tan\theta \quad (86)$$

Taking 0.6 and 0.05 as typical values of C_τ and h/λ, respectively, the primary flow contribution to the factor in brackets in eqn. (85) amounts $0.69\sin^2\theta$ and the secondary flow contribution becomes $-0.21\sin^2\theta+0.016$. The multiplication factor of $\tan\theta$ in eqn. (86) equals 5.5 in that case, which means that for $\theta=5°$, $\alpha=26°$ (i.e. the representative velocity vector deviates 64° from the longshore direction), and for $\theta=30°$, $\alpha=72°$ (i.e. still a deviation angle of 18° with respect to the longshore direction). This leads to the conclusion, that even for large angles of wave incidence the wave-induced secondary current has a substantial influence on the magnitude and the direction of the nearshore current velocity.

As an illustration of the role of these secondary currents, Fig. 11 gives the combined nearshore current velocity for a few salient points at Leadbetter Beach and at Egmond, at various vertical positions. The incident wave conditions for these cases are as given in Table 4.

Moreover, in Fig. 11 an interesting result is given for the horizontal velocity vector at several vertical positions from the TOW-campaign on 17 Nov., 1982 at Egmond beach. This result for one specific location in the surf zone was produced to investigate the feasibility of simultaneous velocity measurements in one vertical. The longshore flow is primarily due to the tidal current and the cross-shore flow is primarily due to the nearly shore-normal wave-breaking. Lack of information on the precise boundary conditions of this situation prevents a comparison with a prediction, but the results of Fig. 11 corroborate the foregoing conclusions. Qualitatively, they also agree with findings from case studies of nearshore morphology (e.g. see Greenwood and Sherman, 1984).

TABLE 4

Incident wave conditions

	H_{rms} (m)	T_p (s)	θ (deg)
T. Pines	0.57	14.3	18.4
Egmond	2.78	8.7	15.0

If the secondary flow strongly influences the near-bottom velocity, it will influence the current-induced sediment transport to roughly the same extent. Hence it must be doubted whether horizontally two-dimensional models of nearshore morphology will ever be able to produce realistic results on the basis of depth-averaged velocities only.

CONCLUSIONS AND FURTHER RESEARCH

The investigations described herein have shown, that is is possible, with the adopted type of turbulence modelling, to combine depth-integrated and verti-

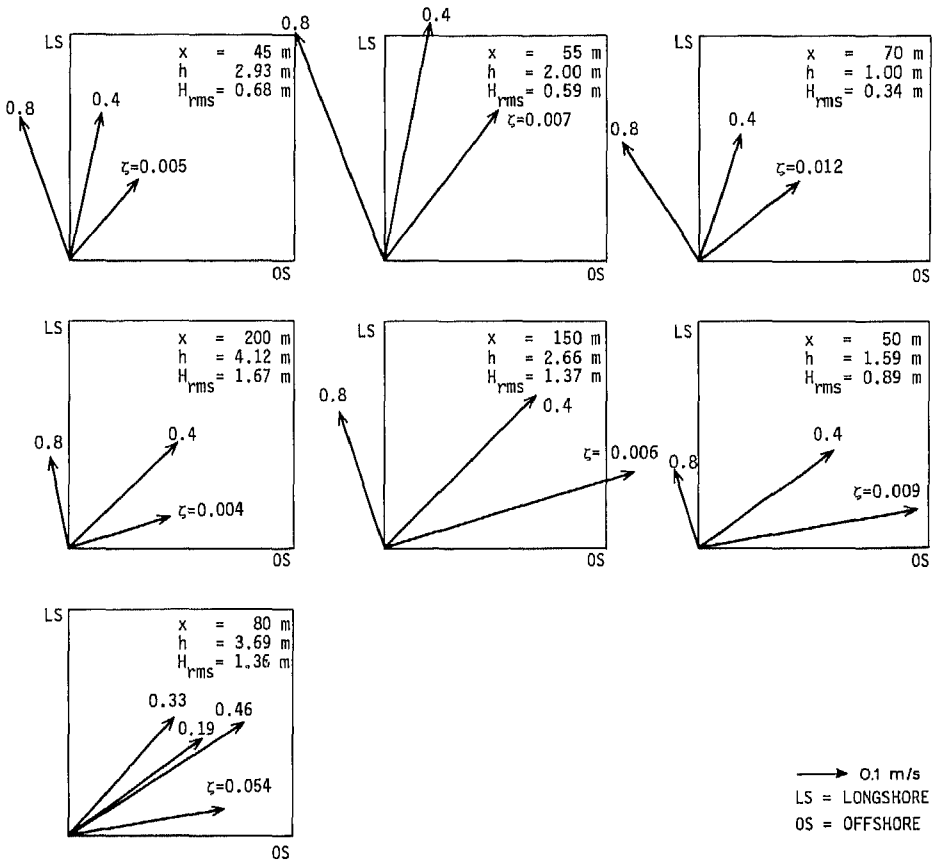

Fig. 11. Nearshore current velocity vector due to primary and secondary flow at selected locations and heights. Top: present model prediction for NSTS-campaign Feb. 4, 1980 at Leadbetter beach; middle: present model prediction for TOW-campaign Dec., 1982 at Egmond beach; bottom: observed velocity vector TOW-campaign 17 Nov., 1982 at Egmond beach induced by alongshore tidal flow and shore-normal wave-breaking (measurements after Derks and Stive, 1984).

cally two-dimensional current models in a consistent manner to a quasi-3D model. From a computational point of view, this model is only a minor extension of the depth-integrated one, which makes it economically attractive. The investigated subsets of this model, describing:
- the vertical distribution of an imposed current in the presence of waves,
- the depth-averaged longshore current velocity along a uniform coast, and
- the undertow in the surf zone at a uniform coast

corresponds well with existing specific models and with measurements from laboratory and field experiments.

The model provides the possibility to estimate the importance of the various components of the wave-induced secondary flow, relative to each other, to the primary velocity and to the effective transport velocities for the cross-shore sediment transport components due to wave asymmetry and bottom slope effects. The mutual comparison of the various components of the wave-induced secondary flow leads to the conclusion, that a random wave field in the surf zone generates important secondary currents (as was found out for monochromatic breaking waves before by many other investigators) and that none of the components of the random wave breaking-induced flow is systematically predominant.

The comparison with the primary current and the effective cross-shore transport velocities reveals that the random wave breaking-induced undertow is always important compared with the wave-induced longshore current velocity and compared with the other cross-shore transport agents in the surf zone. These results indicate that horizontally two-dimensional mathematical models of nearshore morphological evolutions are not likely to be able to produce realistic results on the basis of depth-averaged velocities only.

The model described herein must be considered as a "first shot", based on rather crude assumptions and simplifications and hence open to substantial improvement. Some essential constituents of the model, such as:
- the turbulence modelling;
- the bottom boundary condition for the primary flow; and
- the boundary conditions for the secondary flow

are more or less generalized elaborations of concepts that have been developed and tested for the isolated phenomena they are claimed to describe. It is quite thinkable that these concepts have to be revised when applied in situations with an arbitrary combination of random waves and turbulent flow. Besides, the model in its present form, with its inconsistent treatment of the bottom boundary layer of the secondary flow, is likely to cause problems in the sediment transport computation when incorporated in a morphological model. So, also from this point of view the model needs further improvement.

This leads to the following suggestions for further research:
- investigation of the interaction of waves and turbulent flow in the vertical plane, including the modelling of turbulence; and, derived from this,

- investigation and mathematical modelling of secondary flows due to other causes (curvature, coriolis);
- incorporation of the coriolis-effect (Ekman-effect) and wind-induced secondary flow;
- comparison of quasi-3D model results with those from fully 3D models (cf. Koutitas and Gousidou-Koutita, 1986).

ACKNOWLEDGEMENT

The investigations underlying this paper were carried out in the Task Group Coastal Morphology of the TOW Coastal Research Programme, financed by the Netherlands Government and conducted jointly by the Ministry of Transport and Public Works (Rijkswaterstaat), Delft Hydraulics and the Delft University of Technology. The authors wish to thank Prof. I.A. Svendsen of the Technical University of Denmark for his stimulating discussions. They are greatly indebted to the many researchers who were so kind as to hand over their draft publications before they had actually been published.

REFERENCES

Asano, T. and Iwagaki, Y., 1984. Bottom turbulent boundary layer in wave-current co-existing systems. Proc. 19th ICCE, Houston, pp. 2397-2413.

Bailard, J.A., 1982. Modelling on-offshore sediment transport in the surf zone. Proc. 18th ICCE, Cape Town, pp. 1419-1438.

Battjes, J.A., 1974. Computation of set-up, longshore currents, run-up and overtopping due to wind-generated waves. Doct. Thesis, Delft Univ. of Technol., 244 pp.

Battjes, J.A., 1983. Surf zone turbulence. Proc. 20th IAHR Congr., Moscow, Seminar on Hydrodynamics of Waves in Coastal Areas.

Battjes, J.A. and Janssen, J.P.F.M., 1978. Energy loss and set-up due to breaking of random waves. Proc. 16th ICCE, Hamburg, pp. 569-587.

Battjes, J.A. and Stive, M.J.F., 1985. Calibration and verification of a dissipation model for random breaking waves. J. Geophys. Res., 90(C5): 9159-9167.

Berkhoff, J.C.W., 1976. Mathematical models for simple harmonic linear water waves; wave diffraction and refraction. Doct. Thesis, Delft Univ. of Technol., 103 pp. (also: Delft Hydr. Lab., Publ. No. 163).

Boussinesq, J., 1868. Mémoire sur l'influence de frottement dans les mouvements réguliers des fluides. J. Math. Pures Appl., 2ème Sér., Tome XIII, p. 413.

Buhr-Hansen, J. and Svendsen, I.A., 1984. A theoretical and experimental study of undertow. Proc. 19th ICCE, Houston, pp. 2246-2262.

Coeffé, Y. and Péchon, Ph., 1982. Modelling of sea-bed evolution under wave action. Proc. 18th ICCE, Capetown, pp. 1149-1160.

Coffey, F.C. and Nielsen, P., 1984. Aspects of wave current boundary layer flows. Proc. 19th ICCE, Houston, Texas, pp. 2232-2245.

Craik, A.D.D., 1982. The drift velocity of water waves. J. Fluid Mech., 116: 187-205.

Dally, W.R. and Dean, R.G., 1984. Suspended sediment transport and beach profile evolution. J. Waterway, Port, Coastal and Ocean Eng., 110(1): 15-33.

Davies, A.M., 1987. On extracting current profiles from vertically integrated numerical models. In: P.P.G. Dyke (Editor), JONSMOD '86. Coastal Eng., 11: 445-477.

De Vriend, H.J., 1977. A mathematical model of steady flow in curved shallow channels. J. Hydraul. Res., 15(1): 37-54.

De Vriend, H.J., 1981. Steady flow in shallow channel bends. Doct. Thesis, Delft Univ. of Technology, 260 pp. (also: Dept. of Civil Eng., Comm. on Hydraulics, No. 81-3).

De Vriend, H.J., 1985b. 2DH mathematical modelling in coastal morphology. Proc. Workshop "European Coastal Zones", Athens, Greece, pp. 2.49-2.66.

De Vriend, H.J., 1986a. Two- and three-dimensional mathematical modelling of coastal morphology: recent developments at the Delft Hydraulics Laboratory. Delft Hydraulics Communication No. 377, 34 pp.

De Vriend, H.J., 1986b. 2DH computation of transient sea bed evolutions. Proc. 20th ICCE, Taipei, R.O.C., pp. 1698-1712.

Derks, H. and Stive, M.J.F., 1984. Field investigations in the TOW study programme for coastal sediment transport in The Netherlands. Proc. 19th ICCE, Houston, pp. 1830-1845.

Dingemans, M.W., Radder, A.C. and De Vriend, H.J., 1987. Computation of the driving forces of wave-induced currents. In: P.P.G. Dyke (Editor), JONSMOD '86. Coastal Eng., 11: 539-563.

Dyhr-Nielsen, M. and Sørensen, T., 1970. Some sand transport phenomena on coasts with bars. Proc. 12th ICCE, Washington, pp. 855-865.

Ekman, V.W., 1905. On the influence of the earth's rotation on ocean currents. Ark. Mat., Astron. Fysik, 2(11): 1-53.

Farmer, R.C. and Waldrop, W.R., 1977. A model for sediment transport and delta formation. Coastal Sediment '77 Symp., Charleston (edited by ASCE, New York), pp. 102-115.

Fleming, C.A. and Hunt, J.W., 1976. Application of a sediment transport model. Proc. 15th ICCE, Honolulu, Hawaii, pp. 1184-1202.

Grant, W.D. and Madsen, O.D., 1979. Combined wave and current interaction with a rough bottom. J. Geophys. Res., 84(CY4): 1797-1808.

Greenwood, B. and Sherman, D.J., 1984. Waves, currents, sediment flux and morphological response in a barred nearshore system. Mar. Geol., 60: 31-61.

Guza, R.T. and Thornton, E.B., 1985. Velocity moments in nearshore. J. Waterway, Port, Coastal and Ocean Eng., 111(2): 235-256.

Jenkins, A.D., 1987. A lagrangian model for wind and wave induced near-surface currents. In: P.P.G. Dyke (Editor), JONSMOD '86. Coastal Eng., 11: 513-526.

Kalkwijk, J.P.Th. and Booij, R., 1986. Adaptation of secondary flow in nearly-horizontal flow. J. Hydraul. Res., 24(1): 19-37.

Koutitas, C. and Gousidou-Koutita, M., 1986. A comparative study of three mathematical models for wind-generated circulation in coastal areas. Coastal Eng., 10: 127-138.

Koutitas, C., Kitou, N. and Katopodi, I., 1985. A model for circulation and sediment transport by winds and waves around groyne systems. Proc. Int. Conf. on Numer. Hydraul. Modelling of Ports and Harbours, Birmingham, U.K., pp. 175-180.

Longuet-Higgins, M.S., 1953. Mass transport in water waves. Philos. Trans. R. Soc., Ser. A, 254: 535-581.

Longuet-Higgins, M.S., 1970. Longshore currents generated by obliquely incident sea waves. J. Geophys. Res., 75: 6778-6801.

Lundgren, H., 1972. Turbulent current in the presence of waves. Proc. 13th ICCE, Vancouver, pp. 623-634.

McAnally, W.H., Letter, J.V., Stewart, J.P., Thomas, W.A. and Brogdon, N.J., 1984. Application of Columbia hybrid modelling system. J. Hydraul. Eng., 110(5): 627-642.

McAnally, W.H., Letter, J.V. and Thomas, W.A., 1986. Two- and three-dimensional modelling systems for sedimentation. Proc. Third Int. Symp. River Sedimentation, Mississippi, U.S.A., pp. 400-411.

Memos, C., 1985. Modifications on wave-induced currents. Proc. Workshop "European Coastal Zones", Athens, pp. 1.22-1.31.
Neuman, G. and Pierson, W.J., 1966. Principles of Physical Oceanography. Prentice Hall, Englewood Cliffs, NJ, 545 pp.
Nielsen, P., 1985. A short manual of coastal bottom boundary layers and sediment transport. Public Works Dept., N.S. Wales, Coastal Eng. Branch, TM 85/1, 56 pp.
Phillips, O.M., 1977. The Dynamics of the Upper Ocean. Cambridge University Press, Cambridge, 336 pp.
Schäffer, H.A. and Svendsen, I.A., 1986. Boundary layer flow under skew waves. Tech. Univ. Denmark, Inst. Hydrodyn. Hydraul. Eng., Progress Rep., 64: 13-23.
Stive, M.J.F., 1985. Cross-shore sediment transport. Proc. Workshop "European Coastal Zones", Athens, pp. 1.11-1.19.
Stive, M.J.F., 1986. A model for cross-shore sediment transport. Proc. 20th ICCE, Taipei, R.O.C., pp. 1551-1564.
Stive, M.J.F. and Battjes, J.A., 1984. A model for offshore sediment transport. Proc. 19th ICEE, Houston, pp. 1420-1436. M.J.F. and De Vriend, H.J., 1987. Quasi-3D nearshore current modelling: wave-induced secondary currents. ASCE Specialty Conf. on Coastal Hydrodyn., Delaware, USA.
Stive, M.J.F. and Wind, H.G., 1982. A study of radiation stress and set-up in the nearshore region. Coastal Eng., 6: 1-25.
Stive, M.J.F. and Wind, H.G., 1986. Cross-shore mean flow in the surf zone. Coastal Eng., 10: 235-340.
Svendsen, I.A., 1984. Mass flux and undertow in a surf zone. Coastal Eng., 8: 303-329.
Svendsen, I.A., 1985. On the formulation of the cross-shore wave-current problem. Proc. Workshop "European Coastal Zones", Athens, pp. 1.1-1.9.
Svendsen, I.A., 1986. Analysis of surf zone turbulence. IAHR Int. Conf. Math. Mod. of Wave Breaking and Wave-induced Currents, Grenoble, France.
Swain, A. and Houston, J.R., 1984. Onshore-offshore sediment transport numerical model. Proc. 19th ICCE, Houston, pp. 1244-1251.
Thornton, E.B. and Guza, R.T., 1986. Surf zone longshore currents and random waves: models and field data. J. Phys. Oceanogr., 16: 1165-1178.
Van Doorn, Th., 1981. Experimental investigation of near-bottom velocities in water waves without and with a current. Delft Hydr. Lab., sept. M1423, 66 pp.
Van Kesteren, W.G.M. and Bakker, W.T., 1984. Near bottom velocities in waves with a current; analytical and numerical computations. Proc. 19th ICCE, Houston, pp. 1161-1177.
Visser, P.J., 1984. Uniform longshore current measurements and calculations. Proc. 19th ICCE, Houston, pp. 2192-2207.